Bulletin of the Seismological Society of America, Vol. 87, No. 5, pp. 1330–1344, October 1997

Crustal Thickness Variations in Southern California from Los Angeles Region Seismic Experiment Passive Phase Teleseismic Travel Times

by Monica D. Kohler and Paul M. Davis

Abstract The goal of the 1993 Los Angeles Region Seismic Experiment (LARSE93) passive phase was to collect waveform data from local and distant earthquakes to study lower crust and upper mantle structural features in southern California, particularly under the San Gabriel Mountains and San Andreas fault. During LARSE93, approximately 88 stations were deployed in a 175-km-long, linear array across the Los Angeles basin, San Gabriel Mountains, and Mojave Desert northeast of Los Angeles. During the four weeks of continuous recording, teleseismic events recorded at each site provided a wide range of ray path backazimuths. The teleseismic events included a number of intermediate-magnitude earthquakes with epicenters in the Aleutian Island, Kamchatka, Kuril Island, mid-Atlantic Ridge, Solomon Island, Japan, Fiji Island, and Chile regions. This experiment was followed by LARSE94, which involved land refraction and deep-crustal seismic reflection profiles from offshore and onshore explosion sources. We have used the joint data sets in this study to distinguish upper crustal features from adjacent lower crustal and upper mantle structures. *P*-wave travel times were determined from 17 teleseisms, and upper crustal residual signatures were removed by incorporating LARSE94 upper crustal velocity model results. Within each backazimuth range, the resulting relative travel-time residuals increase from negative values (-0.5-sec average) recorded in the northern San Gabriel Valley–southern San Gabriel Mountain foothills to positive values (0.2-sec average) in the central and northern San Gabriel Mountains. The residual patterns display variations for different backazimuths and incidence angles but show almost no lateral spatial shift of maximum or minimum residual along the array, indicating that the dominant source of the residual pattern is shallow (<50 km). The patterns of residuals require a sharp lateral gradient in shallow velocities between the northern San Gabriel Valley (located in the northernmost Los Angeles basin) and the San Gabriel Mountains over a distance of less than 50 km. Most of the residual pattern can be explained by laterally varying crustal thickness and a high-velocity anomaly in the upper mantle. In our model of Moho depth variations, the northern San Gabriel Valley to the southwest of the array is underlain by thinned continental crust. Crustal thickness increases laterally by 12 km over a distance of less than 50 km into the San Gabriel Mountains. This conclusion is supported by widespread surface evidence for rift-style volcanism and crustal extension in southern California crustal rocks.

Introduction

The Los Angeles basin is surrounded by three distinct physiographic regions: the east–west-trending Transverse Ranges to the north, the northwest–southeast-trending Peninsular Ranges to the southeast, and the continental borderland to the west. These regions are characterized by metamorphosed sedimentary, volcanic, and intrusive basement rocks and are thought to share the same island-arc system source (Wright, 1991). The Los Angeles basin includes the southern foothills of the San Gabriel Mountains and is a Miocene depositional basin with widely varying sedimentary thickness and lithology (Yerkes *et al.*, 1965). The high-angle, reverse San Gabriel frontal fault segment of the Sierra Madre–Cucamonga fault system defines the southern base of the San Gabriel Mountains. It dips northward into the San Gabriel Mountains' granitic and metamorphic rocks and is adjacent to unconsolidated alluvial fan deposits lying to the

south, characterizing the northern San Gabriel Valley (Yerkes *et al.,* 1965). The Los Angeles basin and Transverse Ranges are composed of markedly different geological blocks. Models of their geological and tectonic histories are most effectively constrained by knowledge of the subsurface transition features between physiographic regions.

During its plate tectonic history, southern California underwent distinct phases of deformation including subduction, rifting and extension, and compression resulting in the present-day shape of the Los Angeles basin and Transverse Ranges. Atwater (1970) proposed the existence of a trench offshore from western North America during the mid-Tertiary accompanying Farallon plate subduction, and the origination of San Andreas strike-slip motion after subduction had ceased. Plate reconstructions (Engebretson *et al.,* 1985) have built on Atwater's tectonic evolution model to describe the mid-Tertiary East Pacific Rise collision with the North American plate. The collision and subsequent crustal extension are supported by geological evidence for mid-Miocene rifting and volcanism (Weigand, 1982; Weigand and Savage, 1993) associated with the opening of a rift basin by extension accompanied by high heat flow (Henyey, 1976). Isotope data of the Conejo volcanics in the Santa Monica Mountains indicate an upper mantle source and show little continental crust contamination (Weigand and Savage, 1993). Crustal extension coincides with episodes of pervasive, clockwise block rotation throughout southeast California and is related to changing Farallon subduction deformation style (Luyendyk, 1991). The Los Angeles basin contains numerous high-angle faults that make up a shattered, brittle crust often associated with crustal thinning and block faulting over a mobile layer such as is thought to occur in the Basin and Range Province. Henyey (1976) observed elevated heat flow in the Los Angeles basin and concluded that if the source was hot lithospheric material under the Los Angeles basin, then upper mantle ductility and the potential for crustal thinning, shearing, and volcanism would be increased.

Lithospheric structure under southern California has been investigated by a variety of techniques. Investigations into upper mantle structure include phase delay time analysis (Hadley and Kanamori, 1977; Walck and Minster, 1982; Hearn and Clayton, 1986), teleseismic *P*-wave travel-time tomography (Raikes, 1980; Humphreys *et al.,* 1984; Humphreys and Clayton, 1990; Zhao *et al.,* 1996), polarization tomography (Hu *et al.,* 1994; Powell and Mitchell, 1994), phase stacking techniques (Richards-Dinger and Shearer, 1997), and local earthquake tomography for crustal and upper mantle structure (Sung and Jackson, 1992; Zhao and Kanamori, 1992; Zhao *et al.,* 1996). The upper mantle tomography studies exhibit a high-velocity anomaly that extends more than 200 km into the mantle under the Los Angeles basin and Transverse Ranges (Hadley and Kanamori, 1977; Raikes 1980; Walck and Minster, 1982; Humphreys *et al.,* 1984; Humphreys and Clayton, 1990; Zhao *et al.,* 1996). Detailed upper crustal structure has been investigated using seismic reflection lines (e.g., Li *et al.,* 1992a,b), local geological constraints (Magistrale *et al.,* 1992, 1996), and local earthquake and explosion arrival-time tomography (Hauksson and Haase, 1997). The lower crust and upper mantle tomographic images use data from the Southern California Seismic Network that has an average station spacing of 20 to 30 km. Thus, they do not have the resolution to image localized variations in Moho depth associated with crustal thinning beneath the Los Angeles basin or thickening from transpression in the San Gabriel Mountains. The high-density station spacing achieved by the 1993 phase of the Los Angeles Region Seismic Experiment allows significantly better resolution in the study of Moho depth variations and local lithospheric velocity structures than larger regional arrays. We will show that teleseismic travel-time residuals from this high-density array can be explained by a combination of the regional high-velocity anomaly in the upper mantle and a local crustal root beneath the San Gabriel Mountains.

The Los Angeles Region Seismic Experiment

To date, LARSE has consisted of two experiments: passive, which took place in fall 1993 (LARSE93), and active, which took place in fall 1994 (LARSE94). LARSE93 (Kohler *et al.,* 1996) was a joint effort involving scientists from the University of California at Los Angeles, the U.S. Geological Survey, the California Institute of Technology, and the University of Southern California. It took place between 11 November 1993 and 16 December 1993 and involved the installation of approximately 88 short-period, three-component, digital seismometers along a southwest–northeast array in southern California. The stations were deployed in a 175-km-long linear array across the Los Angeles basin, San Gabriel Mountains, and Mojave Desert (Fig. 1). Seismograms were recorded from local, regional, and teleseismic earthquakes; the teleseismic data were used in this analysis. Azusa was chosen as the starting point of the high-density array because it marks the transition from the high noise of the Los Angeles basin to the low noise in the mountains and desert. Four stations were placed in the central Los Angeles basin (two near Seal Beach and two near Whittier), but the signals recorded at these stations contain relatively high noise levels. As a result, they were not included in this analysis because unambiguous phase travel-time picks could not be determined. The next few stations were in the San Gabriel River fan (in the northern San Gabriel Valley and at the San Gabriel Mountain front) and in the San Gabriel Canyon (in the southern San Gabriel Mountain foothills). The densest part of the array was located in the San Gabriel Mountains with 1-km average spacing; the less dense part, in the Mojave Desert, had 2-km average spacing. A few stations were added to the array during the course of the experiment, and, except for the first few and last few days of the experiment, most stations recorded data continuously during the 4 weeks. One station was located on the San Andreas fault.

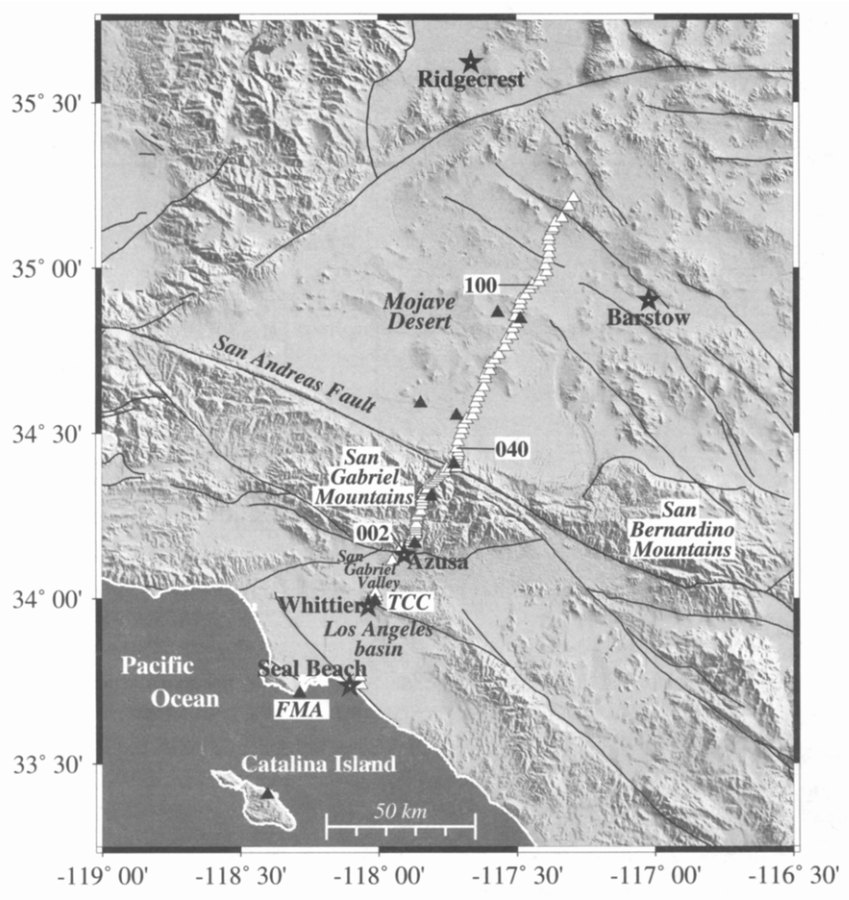

Figure 1. Shaded relief and fault map of southern California showing locations of LARSE93 stations (open triangles) and nearby Southern California Seismic Network (SCSN) stations (filled triangles). Stars mark the locations of cities. Several station names are given for reference (e.g., "040"); station 002 is used as the distance origin in most of the following figures.

The seismograms collected during LARSE93 were complemented by the acquisition of deep-crustal multichannel seismic-reflection and refraction profiles using onshore and offshore sensors, and air-gun and explosion sources (LARSE94: active phase). The data were from ocean-bottom seismometer recording (ten Brink *et al.,* 1996a), onshore recording of air gun shots (Okaya *et al.,* 1996a), onshore recording of earthquake data (Okaya *et al.,* 1996b), deep-crustal seismic-reflection profiles from offshore air-gun sources (Brocher *et al.,* 1995), and LARSE94 explosion survey work (Murphy *et al.,* 1996). We used an upper crustal velocity model determined from inversions of explosion-source *P*-wave travel times along the same line (Lutter and Thurber, 1995; Fuis *et al.,* 1996) to remove travel-time variations due to heterogeneous upper crust.

Teleseismic Travel-Time Analysis

The bulk of LARSE93 data were collected from 13 November 1993 to 11 December 1993. During the 4 weeks of continuous recording, stations recorded waveform data from several hundred teleseismic, regional, and local events. According to the Preliminary Determination of Epicenters (PDE) Catalog produced by the USGS National Earthquake Information Center (NEIC), approximately 140 teleseismic events occurred during this period. Of these, about 20 display useful *P*-wave arrivals from which travel times could be determined. These events fell into several distinct back-azimuth groups with distances between sources and receivers ranging from 30° to 90°. The events included a number of intermediate-magnitude earthquakes with epicenters in the Aleutian Island, Kamchatka, Kuril Island, mid-Atlantic Ridge, Solomon Island, Japan, Fiji Island, and Chile regions. Relative *P*-wave travel times were determined interactively with computer software that recorded the absolute time corresponding to the maximum amplitude of the first visible upswing or downswing chosen by hand. Waveform features were highly coherent across the array.

Profiles of record sections from the array are similar for events within similar backazimuth ranges, and trace quality depends on the station location. Stations in the San Gabriel Mountains and Mojave Desert display higher signal-to-noise ratios than stations in the Los Angeles basin. Two high-quality teleseismic record-section profiles from which *P*-wave travel times were obtained are shown in Figure 2 to illustrate the quality of the data for two different source regions. They are vertical-component velocity seismograms for events that occurred in the Unimak Island region (Fig. 2a) and south of the Fiji Islands (Fig. 2b). The seismograms have been bandpass filtered for frequencies between 0.1 and 1.0 Hz; although there should be seismic energy at higher frequencies, the addition of higher-frequency waveform en-

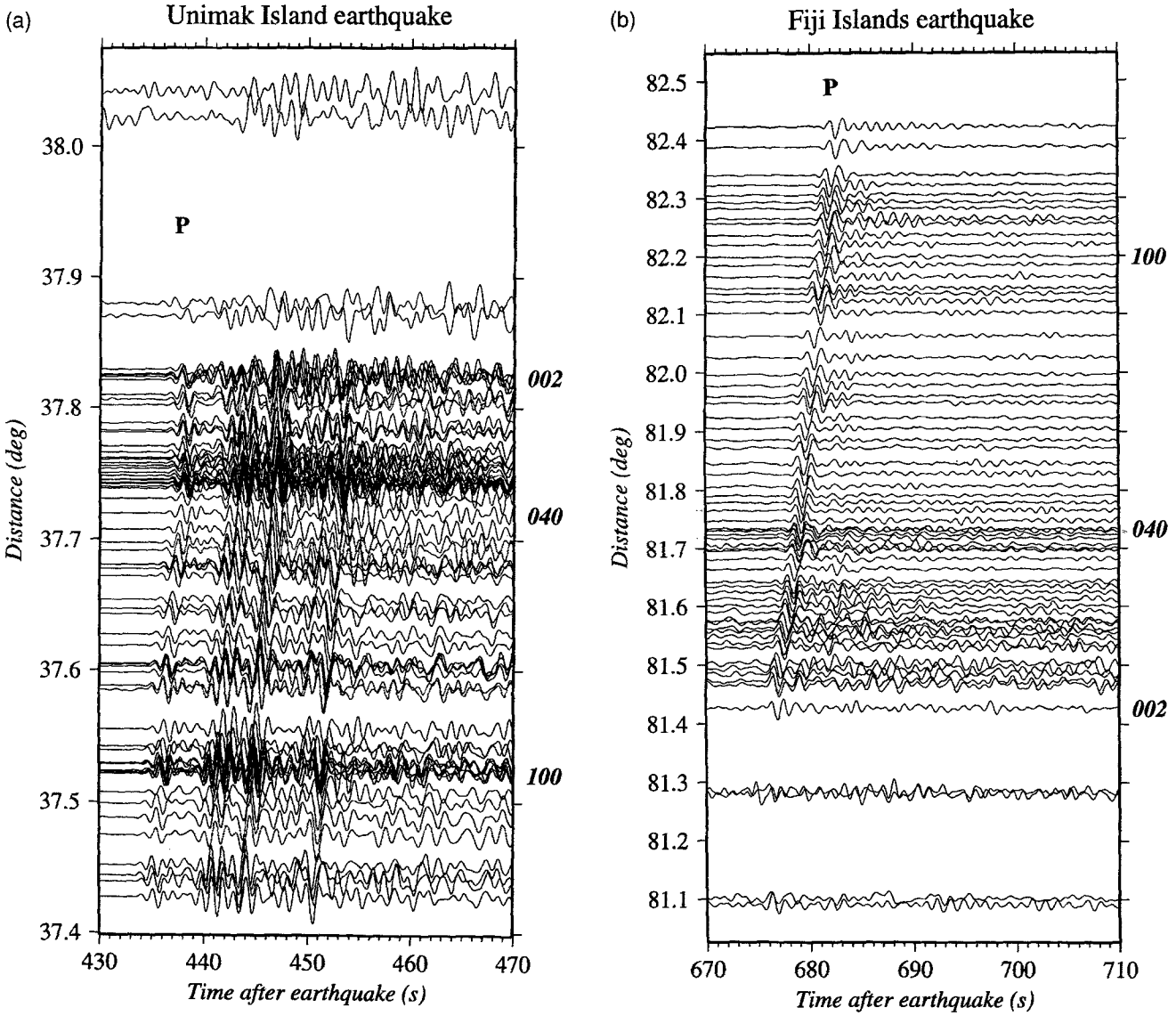

Figure 2. Vertical-component velocity record sections for teleseismic events that occurred on 19 November 1993 (a) in the Unimak Island Region and (b) south of the Fiji Islands. Most Los Angeles basin station recordings have been removed. The seismograms were bandpass filtered for frequencies between 0.1 and 1.0 Hz. Absolute (unreduced) time after earthquake is shown. Selected station names appear to the right of corresponding seismograms (see Fig. 1).

ergy includes signals that obscured the phases. The initial *P* wave is often the best recorded phase at the quiet mountain stations. The noisier Los Angeles basin stations were usually too noisy to obtain phase arrival times.

P-wave travel-time residual curves for stations along the array have been calculated for 17 teleseismic events (Fig. 3, Table 1). *P*-wave travel-time residuals were determined for each station by subtracting one-dimensional Earth model IASP91 travel times (Kennett and Engdahl, 1991) from our picked travel times. Within each backazimuth group, the resulting demeaned travel-time residual curves display consistent patterns. Relative residuals increase from negative values in the northernmost San Gabriel Valley and southern San Gabriel Mountain foothills to positive values in most of the central and northern San Gabriel Mountains, including the San Andreas fault (Fig. 4 with topography effects removed). The largest range in residuals, occurring for ray paths from the northwest (Kamchatka, Unimak Island, and Alaska), is about 1 sec. One event was chosen from each backazimuth group for the inversions in order to avoid a system of equations in which heavily represented regions that have nearly identical travel-time curves (e.g., Aleutian Islands) would dominate the solution (Table 1: entries marked with an asterisk). The sampling distribution is relatively limited in

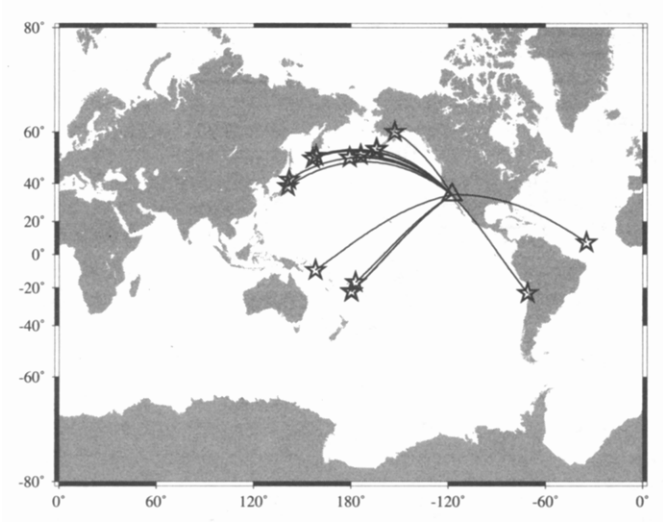

Figure 3. Locations of the earthquakes used in this analysis. The events fall into eight backazimuth groups providing a range of ray-path arrival directions.

backazimuth range due to the short data collection period (e.g., no arrivals from the northeast). However, fine-scale structural features not seen in larger regional network data can be resolved by the high density of data recording.

When obliquely incident rays travel through an anomaly at depth, the pattern of residuals recorded at the surface reflects the shape and depth of the anomaly, and depends on the angles of incidence and backazimuth. The parallax shift is a measure of the surface offset of the residual patterns due to rays arriving from different earthquakes and can be used to estimate the depth of the anomaly when the angles of incidence and backazimuth are known. The LARSE93 teleseismic residual curves display consistent variations for different backazimuths (see Table 1) and incidence angles that range from 15° to 28°, but they show very little parallax shift of residual peaks and troughs (Fig. 5). This indicates that the source of the large residual range is most likely shallow. We estimate that the average depth of the anomaly causing the steep gradient in the southwestern arrivals is less than 50 km when we consider that rays arriving from the north and south with similarly small incidence angles produce residual patterns with a parallax shift of less than 50 km. If the anomaly were deeper, the parallax shift would be greater.

Topographic corrections, using an average crustal velocity of 5.5 km/sec and appropriate incidence angles, did not account for much of the total observed residuals (Fig. 6). The patterns of our residuals are consistent with data shown in Raikes (1980), who interpreted the source of residual variations in terms of upper mantle velocity heterogeneity alone. The residual patterns suggest that, in addition, a sharp lateral gradient in shallow velocities exists beneath the northern San Gabriel Valley–southern San Gabriel Mountain foothills, and the northern San Gabriel Mountains over a distance of less than 50 km. The best fit to the residual data is provided by a crustal thickness model in which the Moho deepens by 12 km beneath the mountains, and overlies a regional upper mantle, high-velocity anomaly similar to that observed previously.

Instead of removing topography travel times before the inversion, rays were projected through an upper crustal *P*-wave velocity model (Lutter and Thurber, 1995; Fuis *et al.*, 1996) to the elevation of each station to remove upper crustal velocity variation signatures from the residuals. The model was produced from the dense reflection–refraction profile along the same line during LARSE94, yielding detailed velocity structure in the upper 10 km of the crust. LARSE94 explosion source intervals were 1 km, and receivers were 100 m apart in the San Gabriel Mountains and 500 m apart in the Los Angeles basin and Mojave Desert. Inversions of first arrivals have yielded velocities with 1.5-km horizontal resolution under the San Gabriel Mountains and 3 km under the Los Angeles basin and Mojave Desert (Lutter and Thurber, 1995). Velocities vary from 2 km/sec at the surface to 6.5 km/sec at 15 to 20 km depth, and depth resolution is best (1 km) in the upper 6 km of the crust. Notable features along this line include a strong reflection possibly originating from the basement ~8 km under the central Los Angeles basin and a low-velocity zone extending as deeply as 6 km under the San Gabriel and San Andreas faults (Fuis *et al.*, 1995, 1996). Images of the upper 2.5 km of the Los Angeles basin region show low velocities (2.0 to 4.0 km/sec); higher upper crustal velocities (4.5 to 6.5 km/sec) occur at the northeastern end of the array, and there is a high-velocity zone dipping to the southwest beneath the San Gabriel Mountains.

The upper crustal velocity corrections applied to our teleseismic residuals functioned both as topography corrections and as station corrections. Removal of these local effects tended to increase the magnitude of the negative residuals due to the near-surface low velocities, and so was unable to explain the residual curves. Much of the observed teleseismic residual still remained after the crustal corrections (Fig. 7).

The final modification we applied to the residuals was removal of the well-documented upper mantle high-velocity anomaly signature (Hadley and Kanamori, 1977; Raikes 1980; Walck and Minster, 1982; Humphreys *et al.*, 1984; Humphreys and Clayton, 1990; Zhao *et al.*, 1996). We chose a simple regional, three-dimensional block representation of the mantle anomaly in which most of it lies beneath the Transverse Ranges and northern Los Angeles basin. Specifically, we represented the mantle anomaly as an east–west-oriented block extending vertically into the mantle whose location was based on the maps shown in Humphreys and Clayton (1990). Travel times were calculated for rays projected through the anomaly (with appropriate angles of incidence and backazimuth) to a depth of 250 km using an average *P*-wave velocity perturbation of 1.5%. Our simple block representation of the mantle anomaly explains the long-wavelength variations of the LARSE93 residual curves satisfactorily because the lateral resolution of these studies

Table 1

Earthquake source data. Origin information is from the Preliminary Determination of Epicenters (PDE) Catalog published by the USGS National Earthquakec Information Center (NEIC). Entries marked with an asterisk were used in the inversions. All events were used in Figures 4 and 5.

Event Location	Coordinates		GMT Time	Depth	Backazimuth	Distance	Magnitude
	Latitude (°N)	Longitude (°E)	(yr:day:hr:min)	(km)	(° clockwise from north)	(°)	(type)
Near east coast of Kamchatka*	51.816	158.659	93:321:11:18	33	314.8	59.9	6.0 (M_w)
Unimak Island region*	54.287	−164.164	93:323:01:43	30	316.2	37.7	6.5 (M_w)
Unimak Island region	54.290	−164.264	93:323:03:22	33	316.2	37.7	4.9 (M_b)
Unimak Island region	54.283	−164.154	93:323:03:58	33	316.2	37.7	5.4 (M_w)
South of Fiji Islands*	−22.427	−179.565	93:323:04:37	591	235.4	81.7	5.3 (M_b)
Central mid-Atlantic Ridge*	7.317	−34.703	93:323:09:05	10	87.9	80.1	5.8 (M_w)
Unimak Island region	54.306	−164.190	93:324:11:54	33	316.3	37.7	5.2 (M_w)
Southern Alaska*	60.025	−153.003	93:324:19:24	116	329.2	34.3	5.9 (M_w)
Kuril Islands	50.747	156.556	93:326:04:16	85	314.1	61.5	5.1 (M_b)
Solomon Islands*	−9.597	158.148	93:330:23:20	17	258.8	90.6	6.2 (M_w)
East coast of Honshu, Japan*	38.625	141.164	93:331:06:11	104	308.0	76.8	5.8 (M_w)
Fiji Islands region	−16.995	−177.048	93:334:20:44	411	237.8	76.0	5.6 (M_w)
Near coast of northern Chile*	−23.205	−70.890	93:335:13:23	33	135.4	72.8	5.3 (M_b)
Aleutian Islands	51.204	179.308	93:337:05:41	33	310.8	47.5	5.6 (M_w)
Hokkaido, Japan region	41.757	141.937	93:338:09:30	84	310.4	74.6	5.2 (M_w)
Aleutian Islands*	52.097	−173.913	93:339:02:36	30	311.8	43.3	5.0 (M_w)
South of Fiji Islands	−22.180	−179.575	93:344:06:31	605	235.6	81.6	5.7 (M_w)

is no better than ~20 km. Because of their lower resolution, however, none of the above models predicts the steep gradients and large ranges seen in the southern and northern San Gabriel Mountain residuals. The mantle anomaly affected the LARSE93 residuals on a length scale comparable to the length of the array.

Forward ray-path travel-time modeling through a recent, relatively high-resolution crustal and upper mantle velocity model (Zhao *et al.,* 1996) indicates that that model lacks the fine-scale, shallow velocity contrasts needed to entirely satisfy the teleseismic residuals. Thus, having taken into account long-wavelength variations due to the mantle anomaly, we are reasonably confident that the short-wavelength variation with its small parallax shift is due to significant crustal thickness variations beneath the LARSE93 array.

Back-Projection Inversion Method

In this section, we quantify the Moho depth variations that would generate the remaining residuals after removal of mantle effects. We apply the downward-projection method (Davis, 1991; Davis *et al.,* 1993) to the teleseismic residuals to obtain a two-dimensional model of a laterally varying interface that separates regions of markedly different velocities. The depth to this interface characterizes crustal thickness from the surface to the Moho discontinuity. This method is useful for obtaining curved-layer structure under a linear array for teleseismic ray paths based on the assumption that the residual patterns are caused primarily by interface undulations. It has the advantage that it is a simple way to determine depth variations of internal boundary layers from initial, horizontally layered velocity structure. It is robust when structural anomalies producing the travel-time residual patterns are shallow compared to the dimensions of the array. Upper crustal travel times are removed from the observed residuals using the straight-ray approximation that is not expected to be significantly different from raytracing through the structure.

The shape of the Moho interface is reflected in *P*-wave travel-time residuals measured at LARSE93 stations. The residual patterns are produced by ray paths traveling obliquely through the curved interface that separates average lower crustal seismic velocities from average upper mantle velocities. The parallax shift in the residual curves is a function of the backazimuth, the incidence angle of the incoming rays, and the depth of the interface. Travel-time residuals are downward projected along incident rays from the station and inverted to obtain the best least-squares fit at the intercept of each ray path with the curved interface expressed as a one-dimensional polynomial in horizontal coordinates.

The travel-time residual calculated for each station can be expressed as a function of upper crustal travel-time residual, source-time offset, upper crustal velocity variation, and crustal thickness,

$$T'_{ij} = \Delta\tau_j + \sum_k a_k X'^k_{ij}, \tag{1}$$

where T'_{ij} are travel-time residuals rotated to vertical incidence for the ith station and jth earthquake, $\Delta\tau_j$ are the earthquake source-time offsets, a_k are polynomial expansion coefficients, and X'^k_{ij} are horizontal coordinates transformed to values projected along the ray path raised to the kth power. The interface is expanded up to a maximum polynomial de-

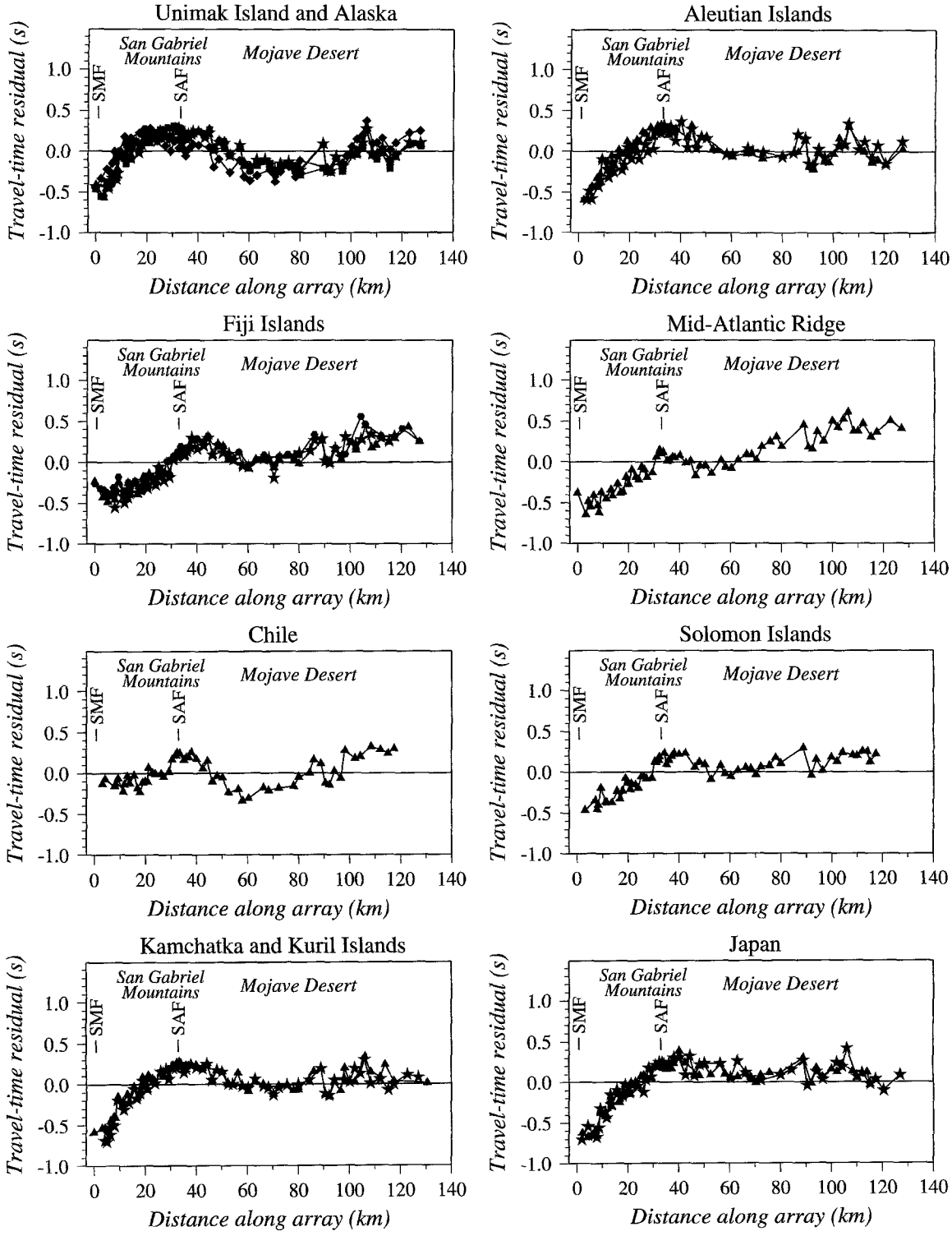

Figure 4. *P*-wave travel-time residual curves for the teleseismic events. Different symbols are used for the different events within each backazimuth group. Distance begins with station 002 (Azusa) at 0 km and increases northeast along the array. The location of the Sierra Madre Fault is indicated by "SMF" and the San Andreas Fault by "SAF." The travel times have been corrected for a one-dimensional Earth model (IASP91) and for topography variations across the array. Note that for most arrivals, especially those from the northwest, residuals are relatively large and negative at the southern end of the array (0 to 20 km) compared to the San Gabriel Mountains (20 to 45 km). Arrivals remain early in the Mojave Desert with more scatter due to errors in instrument clock timing. Mean residuals have been removed individually from each curve.

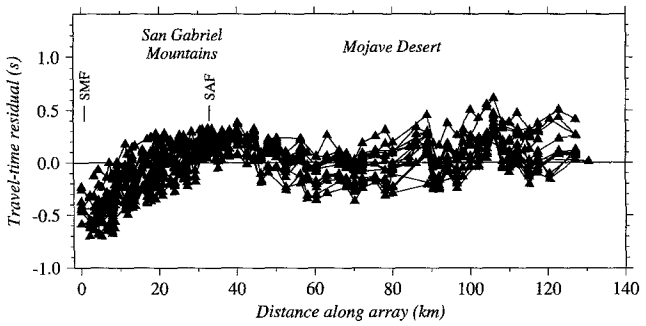

Figure 5. Travel-time residual curves plotted together (with individual means removed). The location of the Sierra Madre Fault is indicated by "SMF" and the San Andreas Fault by "SAF." Distance begins with station 002 (Azusa) at 0 km and increases northeast along the array. Note that the curves do not exhibit a large parallax shift, indicating that the source of the large (up to 1 sec) anomalies is most likely shallow (uppermost mantle and lower crust).

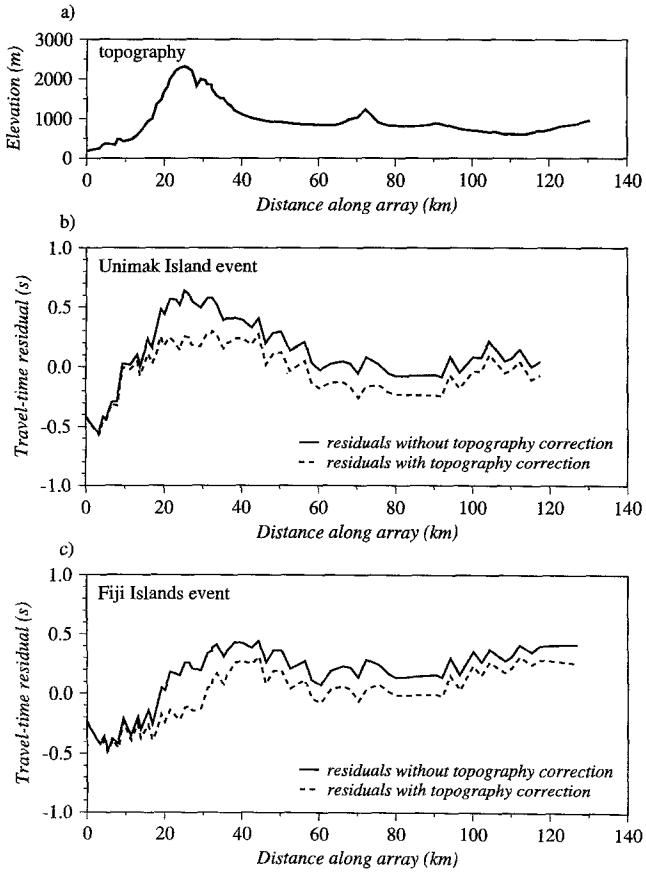

Figure 6. (a) Array elevation and (b,c) travel-time residual curves with and without array topography correction for earthquakes described in Figure 2.

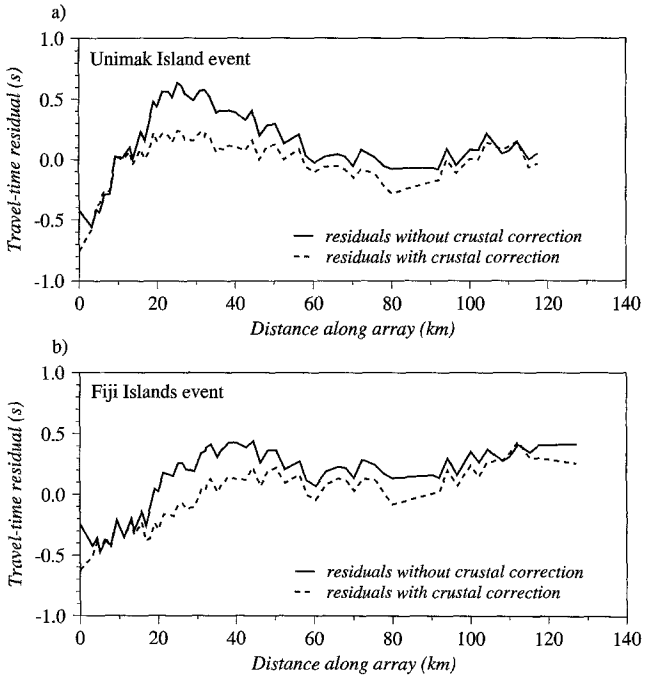

Figure 7. (a,b) Travel-time residual curves with and without LARSE94 upper crustal lateral velocity correction for earthquakes shown in Figure 2.

gree of 6, and the baseline shift is given by the a_0 term. The vertically projected travel times are related to the computed travel times by

$$T'_{ij} = T_{ij} \cos I_{ij}, \tag{2}$$

where I_{ij} is the ray angle of incidence and

$$T_{ij} = T^t_{ij} - T^c_{ij}, \tag{3}$$

where T^t_{ij} are the total observed residuals computed for the oblique rays and T^c_{ij} are the residual contributions from the LARSE94 upper crustal model. Values for T^t_{ij} are obtained by projecting the rays through this model between true station elevation and a depth of 10 km, a depth range in which the resolution of the LARSE94 upper crustal model is the best based on the refraction profile ray-path coverage.

The horizontal coordinates, projected along the ray path to find its intercept with the Moho interface, are given by

$$X'_{ij} = X_i + D_0 \tan I_{ij} \sin(\theta_{ij} - \phi) - AT_{ij} \sin I_{ij} \sin(\theta_{ij} - \phi), \tag{4}$$

where X_i is the horizontal coordinate of the ith station (the X axis is defined along the array), D_0 is the initial mean depth of the interface, θ_{ij} is the backazimuth of the ray, ϕ is the angle between the array and the east–west direction, and velocity factor $A = v_1 v_2/(v_1 - v_2)$; v_1 is the average velocity above the interface and v_2 is the average velocity below.

The data equations were augmented by *a priori* equations that helped constrain the inversion (Jackson, 1979). *A priori* data equations were defined by initial estimates of parameters and corresponding standard deviations that represented the error in the initial estimate. The inversion was solved using a combination of the Marquardt method (Bevington and Robinson, 1992) and *a priori* equations. The values of the *a priori* data covariance matrix coupled with the constant diagonal factors acted as damping parameters; larger standard deviations resulted in more lightly damped, less constrained inversions and smaller, final root mean square (rms) values that represented the agreement between data and model. The *a priori* equations for velocity factor, mean depth, and the event offsets with their standard deviations are given by

$$A = A_0 \pm \sigma_A, \tag{5}$$

$$D = D_0 \pm \sigma_D, \tag{6}$$

and

$$\tau_j = (\tau_j)_0 \pm \sigma_\tau \tag{7}$$

with initial values indicated by subscript 0. The values for σ_A and σ_D were varied to produce a range of models whose parameters and rms values were examined. The expansion coefficients were not explicitly constrained in any of the inversions. Source-time offset terms were added in case there were variations in travel times due to errors in source parameters. The augmented equations were inverted for velocity factor A, expansion coefficients a_k, mean depth D given by $A \cdot a_0$, and event offsets τ_j. The initial interface structure was composed of uniformly small expansion coefficients and was nearly horizontal as a result. This choice of initial coefficient values was intended to allow the higher-order expansion coefficients to converge to any possible solution without starting with a model that was close to an expected final model.

Results—Moho Depth Variations

The final solution was most sensitive to values in A and σ_A, and the final model represents a trade-off between values for A and the interface depth range (given by the polynomial expansion coefficients). Thus, our choice of final model depends on the values we expect for v_1 and v_2, the average lower crustal and upper mantle velocities. Model results are shown in Table 2 and illustrate this trade-off for six cases: v_1 = 6.3, 6.5, or 6.7 km/sec combined with v_2 = 7.8 or 8.0 km/sec. The final rms values were almost the same for the six cases (Table 2). The inversions usually converged within five iterations, and the largest variance reduction occurred after the first iteration. The pattern of interface structure did not depend on the initial assumptions and remained uniform for all inversions reflecting the structure seen in the traveltime residuals.

The depth to the interface $D(X)$ beneath the X axis produced by the inversion results is given by

$$D(X) = A \times \left(\sum_k a_k X^k \right). \tag{8}$$

As Table 2 shows, the corresponding interface depth difference (maximum − minimum depth) between the San Gabriel Valley and San Gabriel Mountains, Δd, varies from 9 to 14 km depending on choice of A. As expected, larger crustal velocities or smaller upper mantle velocities required larger interface depth variations to explain the residuals. Varying the initial value for average depth raised or lowered the range of interface depths by a corresponding amount, but there was almost no control over the final values for average depth; that is, a large range of mean depths produced equally good fits to the data. We examined the depth ranges (Table 2: columns 6 and 7) resulting from two possible maximum Moho depths beneath the San Gabriel Mountains: 30 and 40 km. The 30-km Moho depth is close to the average for southern California and is based on regional studies that find little or no root beneath the San Gabriel Mountains (Kanamori and Hadley, 1975; Hearn, 1984; Hearn and Clayton, 1986). We prefer the model based on the 40-km root because the deeper Moho is suggested by reflectors appearing in high-resolution LARSE94 reflection–refraction profiles along the same line (Ryberg *et al.*, 1996; Hafner *et al.*, 1996).

The remainder of the discussion is based on the results for the case in which v_1 = 6.5 km/sec and v_2 = 7.8 km/sec (Table 2: row 2). The choice of 7.8 km/sec for the average upper mantle velocity is taken from a large number of studies that indicate low average subcrustal velocities beneath the Los Angeles basin and San Gabriel Mountains (Roller and Healy, 1963; Kanamori and Hadley, 1975; Hadley and Kanamori, 1977; Hearn, 1984; Hearn and Clayton, 1986; Richards-Dinger and Shearer, 1997). There is less agreement on the average lower crustal velocity for this region. Our choice of 6.5 km/sec is based on average values given in Hadley and Kanamori (1977), Lutter and Thurber (1995), and Ryberg *et al.* (1996). The velocities are close to the average *P*-wave velocity estimates for continental crust reported by Christensen and Mooney (1995). Our general discussion of the depth variation and its interpretation will be the same regardless of the average interface depth or velocity values.

The results of our inversion are shown in Figure 8 (solid line representing Moho), which illustrates the two-dimensional Moho depth geometry beneath station 002 near Azusa at the southwestern end to the Mojave Desert at the northeastern end. The Moho dips north-northeast beneath the San Gabriel Mountains and deepens by 12 km. The dashed Moho in Figure 8 is an estimate of Moho depth beneath the central Los Angeles basin based on a linear interpolation between measured offshore values (ten Brink *et al.*, 1996b) and our

Table 2

Moho model results. v_1 is the average lower crust P-wave velocity, v_2 is the average upper mantle P-wave velocity, A is the velocity factor $A = v_1v_2/(v_1 - v_2)$, rms is the final root mean square, and Δd is the Moho depth difference between the northern San Gabriel Valley–southern San Gabriel Mountain foothills and the San Gabriel Mountains. Depth range (1) values are the absolute Moho depths assuming a maximum Moho depth of 30 km beneath the mountains, and depth range (2) assumes a maximum Moho depth of 40 km beneath the mountains. Our preferred model is given in row 2 with depth range (2) values.

Model Results						
v_1 (km/sec)	v_2 (km/sec)	A (km/sec)	rms (sec)	Δd (km)	Depth Range (1) (km)	Depth Range (2) (km)
6.3	7.8	−32.8	0.12	9.8	20.2–30.0	30.2–40.0
6.5	7.8	−39.0	0.12	11.7	18.3–30.0	28.3–40.0
6.7	7.8	−47.5	0.12	14.1	15.9–30.0	25.9–40.0
6.3	8.0	−29.7	0.12	8.9	21.1–30.0	31.1–40.0
6.5	8.0	−34.7	0.12	10.4	19.6–30.0	29.6–40.0
6.7	8.0	−41.2	0.12	12.3	17.7–30.0	27.7–40.0

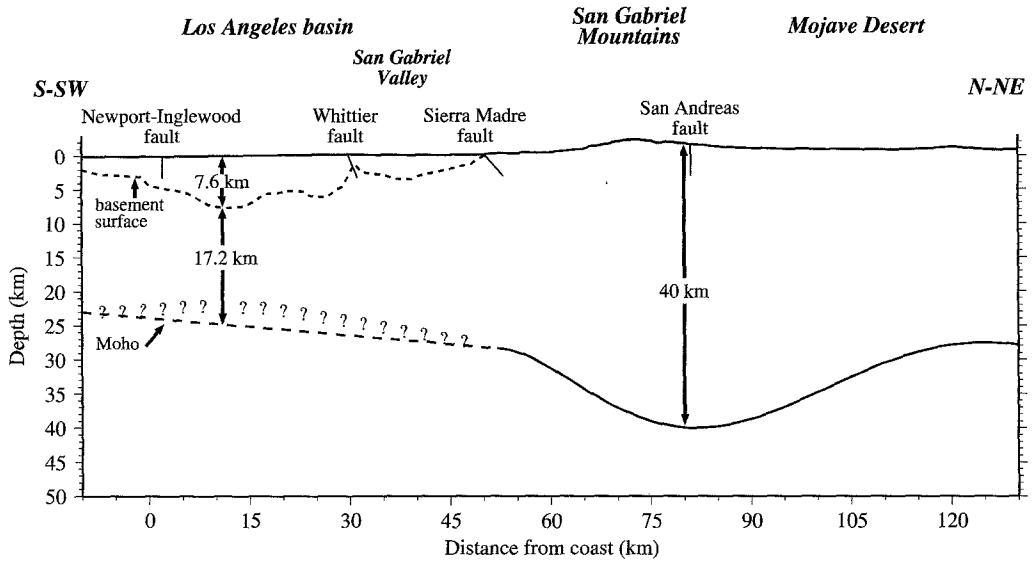

Figure 8. Cross section beneath array showing crustal thickness variations. Moho depth variations resulting from our inversion of the teleseismic travel times are shown by the solid line. The Moho depth difference between the northern San Gabriel Valley–southern San Gabriel Mountain foothills, and the San Gabriel Mountains is 11.7 km. This model assumes a fixed maximum Moho depth of 40 km beneath the San Gabriel Mountains, an average lower crustal velocity of 6.5 km/sec, and an average upper mantle velocity of 7.8 km/sec. The dashed Moho is an estimate of Moho depth beneath the central Los Angeles basin based on a linear interpolation between measured offshore values (ten Brink *et al.*, 1996b) and our results for the northern edge of the basin. The curve composed of question marks represents our best guess of possible Moho upwarp based on our analysis of teleseismic travel times from Southern California Seismic Network stations (described in Discussion section). Fault locations and dips are approximate. The depth to basement surface is from Yerkes *et al.* (1965).

results for the northern edge of the basin. The curve composed of question marks represents our best guess of possible Moho upwarp based on our analysis of teleseismic travel times from Southern California Seismic Network stations, which are described in the next section of this article. The depth to basement surface shown in Figure 8 is from Yerkes *et al.* (1965). The deepest part of the Moho occurs beneath the central segment of the San Gabriel Mountains. The rms misfit between observed and modeled travel times after five iterations was 0.12 sec, which is comparable to a measurement error of 0.1 sec. As a result of a combination of picking accuracy and instrument timing problems, the measurement error is 0.2 sec in the Mojave Desert, which explains the greater individual misfits at those stations.

The two-dimensional polynomial Moho depth model combined with the upper mantle high-velocity anomaly explains most of the crust-corrected travel-time residual data well. Whereas a homogeneous lithosphere produces no re-

sidual, the final model of lithospheric heterogeneity explains most of the residuals for the different backazimuth and distance ranges. We tested the final model (Moho depth variations and upper mantle high-velocity anomaly) by tracing straight rays through it and calculating the predicted travel-time residual at each station, accounting for the LARSE94 upper crustal velocities. The fits for the heterogeneous lithospheric model indicate that it reproduces many distinctive features in the travel-time residual curves (Fig. 9), including the large, negative northern San Gabriel Valley–southern San Gabriel Mountain foothills residuals and the large, positive San Gabriel Mountain residuals. The average data variance reduction computed for all the residual curve fits was 72% (the average variance reduction for inversions that used residuals not corrected for the upper mantle high-velocity anomaly was 54%). As mentioned, the individual travel-time fits to Mojave Desert residuals are not as good because the timing devices of several desert stations were unreliable, producing larger scatter within an individual residual curve; however, trends within backazimuth groups are still predicted.

Discussion

The LARSE experiment was unique in that multiple seismic techniques were used along a finely spaced (1 to 2 km)

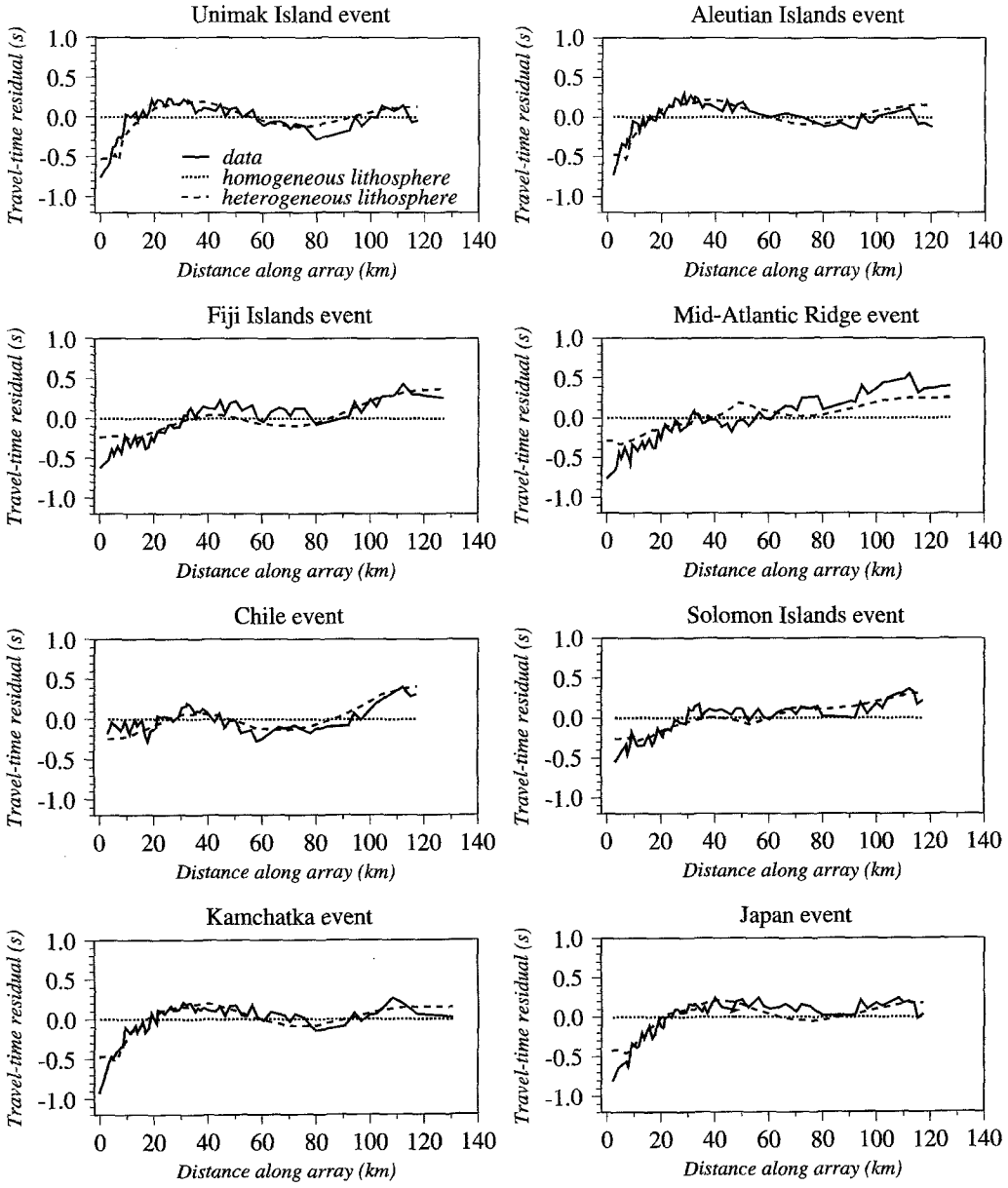

Figure 9. Fits to the travel-time curves for an earthquake in each backazimuth group using a near-horizontal initial model (homogeneous lithosphere) and the final model shown in Figure 8 (heterogeneous lithosphere).

profile in southern California to obtain detailed crustal and upper mantle velocity structure. These included passive recording of teleseisms, regional, and local earthquakes at the 88 stations of the LARSE93 array, active recording of some 60 shots in boreholes on about 600 stations, onshore–offshore recording of air-gun blasts, and offshore OBS recordings. LARSE93 produced a complementary dataset to that of LARSE94 in that it provided deeply penetrating rays that sampled lower crustal and upper mantle structure in southern California.

Relative teleseismic *P*-wave travel-time residuals computed for LARSE93 stations increase from negative values in the northernmost San Gabriel Valley to positive values in the San Gabriel Mountains, including the San Andreas fault. The residuals, which cannot be explained by LARSE94 upper crustal velocity models or by previously derived teleseismic tomography images alone, may be due to large horizontal variations in lower crustal velocity or variations in crustal thickness. The most plausible explanation for the residuals is the effects of shallow mantle under the northern San Gabriel Valley and southern San Gabriel foothills. The large (up to 1 sec) residual differences across the southernmost 50 km of the array are explained as the result of a transition from thinned continental crust under the northern San Gabriel Valley and southern San Gabriel foothills to thicker continental crust under most of the San Gabriel Mountains with a depth difference of 12 km (assuming *P*-wave velocities of 6.5 km/sec above and 7.8 km/sec below the Moho). Using teleseismic receiver functions, Langston (1989) found a major discontinuity dipping north at moderate angles beneath the San Gabriel Mountains 20 km west of the LARSE93 array but placed it in the lower crust. Our approach is relatively simple considering the complex geological and geophysical features exhibited in the LARSE93 array region, but it is a straightforward way to interpret the steep gradient and large range in the teleseismic residuals and is supported by geologic evidence and refraction data.

A significant root beneath the San Gabriel Mountains segment of the Transverse Ranges has not been documented even though the Transverse Ranges appear to be in regional isostatic equilibrium (Oliver, 1980). Although the Bouguer gravity contours over the Transverse Ranges have similar geometry to the average elevation contours, the correlation is not as good in the Mojave Desert where the lowest gravity values occur in an area of moderate elevation (Oliver, 1980). The gravity signature is further complicated by the presence of the upper mantle high-velocity anomaly beneath the Transverse Ranges with its associated density contrast. This has led to the conclusion that the Transverse Ranges are regionally compensated by a very stiff, elastic plate and do not have a substantial crustal root (Sheffels and McNutt, 1986). Our results, however, suggest Airy-type compensation beneath the San Gabriel Mountains.

Travel times determined from nearby Southern California Seismic Network (SCSN) stations suggest that the pattern of early arrivals continues into the central Los Angeles basin. We obtained hand-picked teleseismic *P*-wave travel-time residuals (~34,000) compiled for earlier western U.S. tomography studies (Raikes, 1980; Humphreys *et al.*, 1984; Humphreys and Clayton, 1990; Humphreys and Dueker, 1994) with the goal of extending our residual analysis into a greater portion of the Los Angeles basin and immediately offshore. The residuals were recorded at more than 700 stations in California for ~400 teleseismic events and corrected for topography and a one-dimensional Earth model. We searched for residuals recorded at SCSN stations that were within 10 km of the LARSE93 array and that had contributed data from the ~400 teleseismic events to this residual set (see Fig. 1: filled triangles). The total number of SCSN stations contributing data with this constraint was 10, including stations lying along the southwestward projection of our array (near Whittier, Seal Beach, and on Catalina Island). Events were isolated for which a pick had been made either at station TCC (near Whittier) or at station FMA (near Seal Beach) (or both) in order to observe the residual variation in the Los Angeles basin; that is, events were discarded if no picks were made for either of these stations. Events were also discarded if only one pick had been made out of the 10 stations for an event. We corrected the SCSN residuals (originally corrected only for topography) for upper crust travel-time variations three different ways: by projecting rays through the upper crustal velocity models of Hauksson and Haase (1997), that of Magistrale *et al.* (1996), and by applying standard SCSN station corrections. The results were very similar for each type of correction and all had the largest effect on the station near Whittier because of shallow, low-velocity material in the region. The limited number of residuals from picks made at basin stations illustrates the continuing difficulty of obtaining high-resolution tomographic images directly beneath a basin with high levels of cultural and seismic noise.

The resulting residual curves (Fig. 10: filled symbols), corrected for topography and upper crustal velocity variations using the model of Hauksson and Haase (1997), have distinct patterns within each range of backazimuths (northwest, southwest, and southeast; there were no events from the northeast that were recorded at either TCC or FMA), but almost all curves display the largest negative residuals for stations TCC and FMA. Moreover, all curves display early arrivals in the Los Angeles basin and late arrivals offshore at the Catalina Island station. (Note that the events recorded by the SCSN stations are different from those listed in Table 1.) A constant time shift was applied to each SCSN residual curve in Figure 10 so that TCC or FMA residuals would be constant among different events. Typical LARSE93 teleseismic residual curves for each quadrant, also time-shifted for comparison, and corrected for topography and upper crustal velocity variations, are plotted as dashed lines in Figure 10. Azusa is the common station between the LARSE93 profiles and the SCSN data.

Thinned crust beneath the central Los Angeles basin due to stretching would produce the observed residual patterns (Fig. 8). Our model is two-dimensional, but the data exhibit

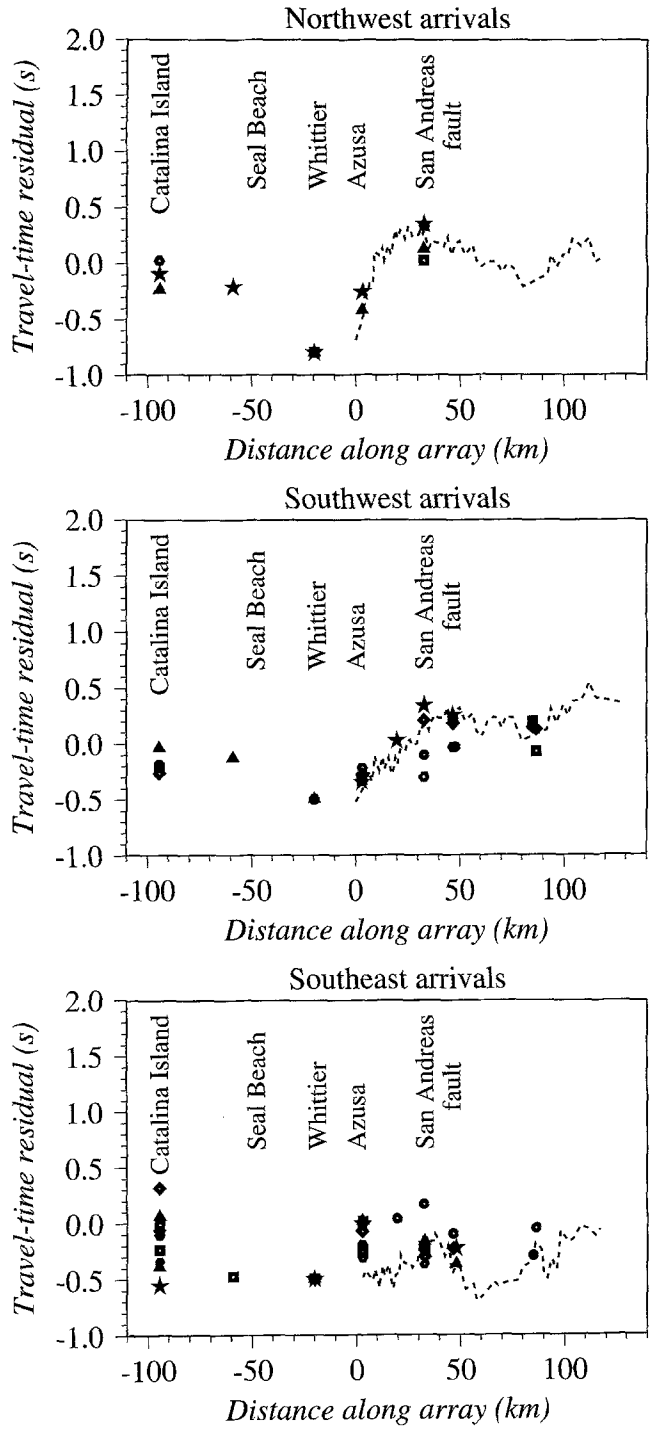

Figure 10. Residual curves for SCSN stations shown in Figure 1 where picks were recorded for events within quadrants shown on top of each plot. Each event is shown by a different symbol, and the events are not the same as those shown in Table 1. Upper crustal velocity variation effects were removed using the *P*-wave velocity model of Hauksson and Haase (1997) [the curves were very similar using the *P*-wave velocity model of Magistrale *et al.* (1996) or standard SCSN station corrections]. A constant time shift was applied to each SCSN residual curve in Figure 10 so that TCC or FMA residuals would be constant among different events. Typical LARSE93 teleseismic residual curves for each quadrant, also time-shifted for comparison and corrected for topography and upper crustal velocity variations, are plotted as dashed lines.

three-dimensional variations due to three-dimensional velocity and crustal thickness heterogeneity not modeled here. The shorter-wavelength (<50 km) variations in residuals are largest for arrivals from the northwest and smallest from the southeast (seen in Figs. 4 and 10) and suggest that the shape of the upwarped Moho is asymmetric. Accounting for differences in angles of incidence and backazimuth, the data suggest that the Moho is shallower and steeper to the northwest than to the southeast.

Our thinned continental crust model is supported by evidence for Los Angeles basin crustal extension during recent tectonic history. After the bulk of Farallon plate subduction ceased ~37 m.y.a., the East Pacific Rise began colliding with the western margin of the continent, and the Pacific and North American plates came into contact (Atwater, 1970). The resulting regime was characterized by volcanism thought to be due to upwelling of lithospheric mantle into the window originally occupied by the subducted slab (Weigand and Savage, 1993). Present-day features began forming around 12 m.y.a. with the subsided Los Angeles basin moving with the Pacific plate as the San Andreas fault system developed to the east (Wright, 1991). Extension gave way to transpression, resulting in the uplift of the Transverse Ranges and the production of blind thrusts beneath the basin (e.g., Wright, 1991; Crouch and Suppe, 1993; Davis and Namson, 1994). Prior to this, volcanism and subsidence marked a well-documented episode of basin rifting. For example, the Conejo volcanic fields in the Santa Monica Mountains are similar to the thickest volcanic sequences in the southern foothills of the San Gabriel Mountains (Glendora Volcanics), Santa Cruz Island, and along the southern margin of the western Transverse Ranges, and are the result of middle Miocene crustal rifting and extension (Wright, 1991). The occurrence of volcanism with rapid subsidence is characteristic of extensional tectonics in pull-apart basins underlain by thinned lithosphere (Mayer, 1987). Crustal extension may have been accommodated by zones of mid-Miocene extensional faulting adjacent to the Los Angeles basin (e.g., the Malibu-Santa Monica-Hollywood fault system) (Wright, 1991) and older high-angle normal faults above major detachments (Crouch and Suppe, 1993).

The development and evolution of sedimentary basins may include rapid stretching of continental lithosphere followed by thinning and asthenosphere upwelling (McKenzie, 1978). In this theoretical model, subsidence accompanies these events, and the amount of stretching can be calculated from the change in crustal thickness (McKenzie, 1978). If

we assume that thinning is inversely proportional to crustal extension, then the amount of extension can be calculated relative to an original, undeformed value. Consider our first case in which the Moho is 40 km deep beneath the mountains and it shallows by 11.7 km (see Table 2) to 28.3 km beneath the northern San Gabriel Valley. Linear extrapolation yields a Moho depth of 24.8 km beneath the central Los Angeles basin where the sediments are the thickest along our profile (see Fig. 8). Hence, the crust has thinned from an average, undeformed 23 km (given by offshore crustal thickness adjacent to the southwest end of our profile) (ten Brink *et al.*, 1996b) to 17.2 km in the basin after subtracting 7.6 km of overlying sediments (Yerkes *et al.*, 1965) (see Fig. 8). This corresponds to a minimum of 34% extension that has occurred between the San Gabriel Mountain crustal block and the Los Angeles basin block. In the more extreme case in which the Moho is 30 km deep beneath the mountains, the crust has thinned from 23 to 7.2 km (again subtracting 7.6 km of sediments). Over 200% extension has occurred. Mayer (1987) and Sawyer *et al.* (1987) used McKenzie's theoretical model to relate Los Angeles basin subsidence to extension and sedimentary thicknesses. Mayer (1987) obtained 50% to 75% lithospheric thinning under the central portion of the Los Angeles basin, and Sawyer *et al.* (1987) calculated 178% extension in the Los Angeles basin along with 20% extension in the adjacent northeast crustal block (which includes the northernmost San Gabriel Valley and southern San Gabriel Mountain foothills). Our values for extension represent a transition from thinned Los Angeles basin continental crust to adjacent thicker San Gabriel Mountains crust.

The high-density LARSE93 array data and residuals from Southern California Seismic Network basin stations are consistent with southern California lithosphere that includes thickened crust beneath the San Gabriel Mountains, a thinned crust beneath the Los Angeles basin, and an upper mantle high-velocity anomaly beneath the Transverse Ranges. The lateral resolution of existing southern California upper mantle velocity models is >20 km, and they are useful for imaging regional velocity structure. The upper mantle high-velocity anomaly produced in several of the models, whose location and resolution is controlled by the Southern California Seismic Network geometry, affects the LARSE93 residuals on a length scale comparable to the dimensions of the array. Although the upper mantle models predict the long-wavelength features of our residual curves, they are too long wavelength to reproduce small-scale details such as the variation in crustal thickness beneath the San Gabriel Mountains. The Los Angeles Region Seismic Experiment passive phase demonstrates how high-density arrays can reveal small-scale lithospheric structure not seen in regional network data.

Acknowledgments

We wish to thank the many scientists without whose help this experiment would have been nearly impossible, in particular, Gary Fuis, Rob Clayton, Dave Okaya, and Jim Mori. Our thanks also go to Marcos Alvarez, Mark Benthien, Joyjeet Bhowmik, Armando Burciaga, Bob Busby, Cheryl Contopoulos, Ed Criley, H. Ekstrom, Jim Fowler, Shangxing Gao, Doug Given, Katrin Hafner, Thomas Henyey, Craig Jones, Brian Laird, Hong Liu, Aaron Martin, Steve Michnik, Janice Murphy, Julie Norris, Guang-yu Pei, Robert Phinney, Michelle Robertson, Craig Scrivner, and John Van Schaak. Many of these scientists, students, and volunteers spent their time in the field deploying and monitoring the array instruments, providing us with instruments and equipment, and providing follow-up maintenance. Our thanks also go to Ken Dueker for supplying us with the large compilation of *P*-wave residual data. Egill Hauksson and Harold Magistrale were kind enough to forward their southern California upper crustal velocity models to us. We are grateful for the thoughtful reviews provided by Marianne Walck and Jennifer Haase that significantly improved our manuscript. This work was supported by the Southern California Earthquake Center (SCEC Contribution Number 352) and the National Science Foundation.

References

Atwater, T. (1970). Implications of plate tectonics for the Cenozoic tectonic evolution of western North America, *Geol. Soc. Am. Bull.* **81,** 3513–3536.

Bevington, P. R. and D. K. Robinson (1992). *Data Reduction and Error Analysis for the Physical Sciences,* McGraw-Hill, San Francisco.

Brocher, T. M., R. W. Clayton, K. D. Klitgord, R. G. Bohannon, R. Sliter, J. K. McRaney, J. V. Gardner, and J. B. Keene (1995). Multichannel seismic-reflection profiling on the R/V Maurice Ewing during the Los Angeles Region Seismic Experiment (LARSE), California, *U.S. Geol. Surv. Open-File Rept. 95-228.*

Christensen, N. I. and W. D. Mooney (1995). Seismic velocity structure and composition of the continental crust: a global view, *J. Geophys. Res.* **100,** 9761–9788.

Crouch, J. K. and J. Suppe (1993). Late Cenozoic tectonic evolution of the Los Angeles basin and inner California borderland: a model for core complex-like crustal extension, *Geol. Soc. Am. Bull.* **105,** 1415–1434.

Davis, P. M. (1991). Continental rift structures and dynamics with reference to teleseismic studies of the Rio Grande and East African rifts, *Tectonophysics* **197,** 309–325.

Davis, T. L. and J. S. Namson (1994). A balanced cross-section of the 1994 Northridge earthquake, Southern California, *Nature* **372,** 167–169.

Davis, P. M., P. Slack, H. A. Dahlheim, W. V. Green, R. P. Meyer, U. Achauer, A. Glahn, and M. Granet (1993). Teleseismic tomography of continental rift zones, in *Seismic Tomography: Theory and Practice,* H. M. Iyer and K. Hirahara (Editors), Chapman and Hall, London.

Engebretson, D. C., A. Cox, and R. G. Gordon (1985). Relative motions between oceanic and continental plates in the Pacific basin, *Geol. Soc. Am. Special Paper 206.*

Fuis, G. S., T. M. Brocher, K. Klitgord, D. A. Okaya, T. M. Henyey, R. W. Clayton, T. Ryberg, and W. J. Lutter (1995). An overview of preliminary seismic images from the Los Angeles Region Seismic Experiment (abstract) *EOS* **76,** F347.

Fuis, G. S., D. A. Okaya, R. W. Clayton, W. J. Lutter, T. Ryberg, T. M. Brocher, T. M. Henyey, M. L. Benthien, P. M. Davis, J. Mori, R. D. Catchings, U. S. ten Brink, M. D. Kohler, K. D. Klitgord, and R. G. Bohannon (1996). Images of crust beneath southern California will aid study of earthquakes and their effects, *EOS* **77,** 173.

Hadley, D. and H. Kanamori (1977). Seismic structure of the Transverse Ranges, California, *Geol. Soc. Am. Bull.* **88,** 1469–1478.

Hafner, K., R. W. Clayton, and E. Hauksson (1996). Mid and lower-crustal structure beneath the San Gabriel Mountains, CA (LARSE) (abstract), *EOS* **77,** F738.

Hauksson, E. and J. S. Haase (1997). Three-dimensional V_p and V_p/V_s velocity models of the Los Angeles Basin and Central Transverse Ranges, California, *J. Geophys. Res.* **102,** 5423–5453.

Hearn, T. M. (1984). Pn travel times in southern California, *J. Geophys. Res.* **89,** 1843–1855.

Hearn, T. M. and R. W. Clayton (1986). Lateral velocity variations in southern California. II. Results for the lower crust from Pn waves, *Bull. Seism. Soc. Am.* **76,** 511–520.

Henyey, T. L. (1976). Heat flow and tectonic patterns on the southern California borderland, in *Aspects of the Geologic History of the California Continental Borderland,* D. G. Howell (Editor), American Association of Petroleum Geologists Miscellaneous Publication 24.

Hu, G., W. Menke, and C. Powell (1994). Polarization tomography for P-wave velocity structure in southern California, *J. Geophys. Res.* **99,** 15245–15256.

Humphreys, E. D. and R. W. Clayton (1990). Tomographic image of the southern California mantle, *J. Geophys. Res.* **95,** 19725–19746.

Humphreys, E. D., R. W. Clayton, and B. H. Hager (1984). A tomographic image of mantle structure beneath southern California, *Geophys. Res. Lett.* **11,** 625–627.

Jackson, D. D. (1979). The use of *a priori* data to resolve non-uniqueness in linear inversion, *Geophys. J. R. Astr. Soc.* **57,** 137–157.

Kanamori, H. and D. Hadley (1975). Crustal structure and temporal velocity change in southern California, *Pure Appl. Geophys.* **113,** 257–280.

Kennett, B. L. N. and E. R. Engdahl (1991). Traveltimes for global earthquake location and phase identification, *Geophys. J. Int.* **105,** 429–465.

Kohler, M. D., P. M. Davis, H. Liu, M. Benthien, S. Gao, G. S. Fuis, R. W. Clayton, D. Okaya, and J. Mori (1996). Data report for the 1993 Los Angeles Region Seismic Experiment (LARSE93), southern California: a passive study from Seal Beach northeastward through the Mojave Desert, *U.S. Geol. Surv. Open-File Rept. 96-85.*

Langston, C. A. (1989). Scattering of teleseismic body waves under Pasadena, California, *J. Geophys. Res.* **94,** 1935–1951.

Li, Y.-G., T. L. Henyey, and L. T. Silver (1992a). Aspects of the crustal structure of the Western Mojave Desert, California, from seismic reflection and gravity data, *J. Geophys. Res.* **97,** 8805–8816.

Li, Y.-G., T. L. Henyey, and P. C. Leary (1992b). Seismic reflection constraints on the structure of the crust beneath the San Bernardino Mountains, Transverse Ranges, Southern California, *J. Geophys. Res.* **97,** 8817–8830.

Lutter, W. J. and C. Thurber (1995). An image of the upper 5 km from inversion of first arrivals from the 1994 LARSE experiment: line 1 from Seal Beach to El Mirage Lake (abstract), *EOS* **76,** F348.

Luyendyk, B. P. (1991). A model for Neogene crustal rotations, transtension and transpression in southern California, *Geol. Soc. Am. Bull.* **103,** 1528–1536.

Magistrale, H., H. Kanamori, and C. Jones (1992). Forward and inverse three-dimensional P wave velocity models of the southern California crust, *J. Geophys. Res.* **97,** 14115–14135.

Magistrale, H., K. McLaughlin, and S. Day (1996). A geology-based 3D velocity model of the Los Angeles basin sediments, *Bull. Seism. Soc. Am.* **86,** 1161–1166.

Mayer, L. (1987). Subsidence analysis of the Los Angeles basin, in *Cenozoic Basin Development of Coastal California,* R. V. Ingersoll and W. G. Ernst (Editors), Prentice-Hall, Englewood Cliffs, New Jersey.

McKenzie, D. (1978). Some remarks on the development of sedimentary basins, *Earth Planet. Sci. Lett.* **40,** 25–32.

Murphy, J. M., G. S. Fuis, T. Ryberg, D. A. Okaya, E. E. Criley, M. L. Benthien, M. Alvarez, I. Asudeh, W. M. Kohler, G. N. Glassmoyer, M. C. Robertson, and J. Bhowmik (1996). Report for the explosion data acquired in the 1994 Los Angeles Region Seismic Experiment (LARSE94), Los Angeles, California, *U.S. Geol. Surv. Open-File Rept. 96-536.*

Okaya, D. A., J. Bhowmik, G. S. Fuis, J. M. Murphy, M. C. Robertson, A. Chakraborty, M. L. Benthien, K. Hafner, and J. J. Norris (1996a). Report for airgun data acquired at onshore stations during the 1994 Los Angeles Region Seismic Experiment (LARSE), California, *U.S. Geol. Surv. Open-File Rept. 96-297.*

Okaya, D. A., J. Bhowmik, G. S. Fuis, J. M. Murphy, M. C. Robertson, A. Chakraborty, M. L. Benthien, K. Hafner, and J. J. Norris (1996b). Report for local earthquake data acquired at onshore stations during the 1994 Los Angeles Region Seismic Experiment (LARSE), California, *U.S. Geol. Surv. Open-File Rept. 96-509.*

Oliver, H. W. (1980). Transverse ranges, in *Interpretation of the gravity map of California and its continental margin,* H. W. Oliver (Editor), *Calif. Div. Mines Geol. Bull. 205.*

Powell, C. A. and B. T. Mitchell (1994). Relative array analysis of the southern California lithosphere, *J. Geophys. Res.* **99,** 15257–15275.

Raikes, S. A. (1980). Regional variations in upper mantle structure beneath southern California, *Geophys. J. R. Astr. Soc.* **63,** 187–216.

Richards-Dinger, K. B. and P. M. Shearer (1997). Estimating crustal thickness in southern California by stacking PmP arrivals, *J. Geophys. Res.* **102,** 15211–15224.

Roller, J. C. and J. H. Healy (1963). Seismic-refraction measurements of crustal structure between Santa Monica Bay and Lake Mead, *J. Geophys. Res.* **68,** 5837–5849.

Ryberg, T., G. S. Fuis, W. J. Lutter, and D. A. Okaya (1996). Mid- and upper-crustal structure of the San Gabriel Mountains: results from the Los Angeles Region Seismic Experiment (abstract), *EOS* **77,** F737.

Sawyer, D. S., A. T. Hsui, and M. N. Toksöz (1987). Extension, subsidence and thermal evolution of the Los Angeles Basin—a two-dimensional model, *Tectonophysics* **133,** 15–32.

Sheffels, B. and M. McNutt (1986). Role of subsurface loads and regional compensation in the isostatic balance of the Transverse Ranges, California: evidence for intracontinental subduction, *J. Geophys. Res.* **91,** 6419–6431.

Sung, L.-Y. and D. D. Jackson (1992). Crustal and uppermost mantle structure under southern California, *Bull. Seism. Soc. Am.* **82,** 934–961.

ten Brink, U. S., R. M. Drury, G. K. Miller, T. M. Brocher, and D. Okaya (1996a). Los Angeles Region Seismic Experiment (LARSE)—offshore seismic refraction data, *U.S. Geol. Surv. Open-File Rept. 96-27.*

ten Brink, U. S., J. Zhang, and J. Loss (1996b). California Borderland crust in relation to the Western Transverse Ranges (abstract), EOS **77,** F737.

Walck, M. C. and J. B. Minster (1982). Relative array analysis of upper mantle lateral velocity variations in southern California, *J. Geophys. Res.* **87,** 1757–1772.

Weigand, P. W. (1982). Middle Cenozoic volcanism of the western Transverse Ranges, in *Geology and Mineral Wealth of the California Transverse Ranges,* D. L. Fife and J. A. Minch (Editors), South Coast Geological Society, Santa Ana, California.

Weigand, P. W. and K. L. Savage (1993). Review of the Petrology and Geochemistry of the Miocene Conejo Volcanics of the Santa Monica Mountains, California, in *Depositional and Volcanic Environments of Middle Tertiary Rocks in the Santa Monica Mountains, Southern California*: P. W. Weigand, A. E. Fritsche, and G. E. Davis (Editors), Pacific Section, Society for Sedimentary Geology, Bakersfield, California, Vol. **72,** 93–112.

Wright, T. L. (1991). Structural geology and tectonic evolution of the Los Angeles basin, California, in *Active Margin Basins,* K. T. Biddle (Editor), *AAPG Memoir 52.*

Yerkes, R. F., T. H. McCulloh, J. E. Schoellhamer, and J. G. Vedder (1965). Geology of the Los Angeles basin California—an introduction, *Geol. Surv. Profess. Pap. 420-A.*

Zhao, D. and H. Kanamori (1992). P-wave image of the crust and uppermost mantle in southern California, *Geophys. Res. Lett.* **19,** 2329–2332.

Zhao, D., H. Kanamori, and E. Humphreys (1996). Simultaneous inversion of local and teleseismic data for the crust and mantle structure of southern California, *Phys. Earth Planet. Interiors* **93,** 191–214.

Department of Earth and Space Sciences
University of California at Los Angeles
Box 951567
Los Angeles, California 90095-1567

Manuscript received 3 September 1996.